

https://dspace.org/

Densification, microstructure and properties of liquidphase sintered silicon carbide materials

Can, Antionette

2006-02-06
http://hdl.handle.net/10539/172

Downloaded from a DSpace repository. https://dspace.org/

4. RESULTS OF HOT PRESSING, GAS PRESSURE SINTERING AND HEAT TREATMENTS

In this part of the thesis, the results for the densification, heat treatments and all the properties testing will be presented. Discussion of these results and of densification-microstructure-properties relationships are given in Chapter 5. Results and discussion of the UHP samples are given in Chapter 6.

4.1 Densification and Heat Treatment

The different previously listed selected compositions were hot pressed (HP), gas pressure sintered (GPS) and ultra-high pressure sintered (UHP). The hot pressed and gas pressure sintered materials were then heat treated for different times at 1925°C and 5 hours at 1975°C. The results for the hot pressing, gas pressure sintering and their post-sintering heat treatments will be presented in this section (4.1).

4.1.1 Densification by hot pressing (HP)

Hot pressing was done using two different pieces of hot pressing equipment (making up the HP-W and the HP materials.) The densities of the hot pressed samples are summarised in Table 4.1.

A comparison of the determined density with the theoretical densities shows that most of the measured densities are between the two calculated theoretical densities $\rho_{theoretical1}$ and $\rho_{theoretical2}$. $\rho_{theoretical1}$ assumes the presence of silica in the sintered material, whereas $\rho_{theoretical2}$ is calculated without taking into account the SiO_2 content (method of calculation of the

theoretical densities can be found in section 3.3.2). The measured densities are closer to the densities calculated under the assumption that the SiO_2 remains in the grain boundaries. XRD results in section 4.2 confirms that the HP samples contain most of the SiO_2 existing in the starting powders. All the hot pressed samples were dense (more than 99 % dense), except for HP1Y4Al_4 and HP0.7YS.

Alumina contamination coming from the milling balls and pot in the HP-W samples was very high and therefore these samples were not studied in as much detail as the remaining HP samples. Some results for the HP-W materials can be seen in Appendix B.

Table 4.1 Densities of hot pressed materials

Sample	**Density (g/cm^3)**	**$\rho_{theoretical1}$ (g/cm^3) (with SiO_2)**	**$\rho_{theoretical2}$ (g/cm^3) (without SiO_2)**	**ρ_1(%)**	**ρ_2(%)**
HP3Y5Al-W	3.27	3.29	3.36	99.4	97.3
HP1Y1Al-W	3.27	3.26	3.33	100.3*	98.2
HP4Y2Al-W	3.29	3.30	3.37	99.7	97.6
HP4Y1Al	3.31	3.30	3.37	100.3*	98.2
HP4Y:2Al	3.30	3.29	3.37	100.3*	97.9
HP1Y1Al	3.27	3.29	3.36	99.4	97.3
HP3Y5Al	3.26	3.28	3.35	99.7	97.3
HP1Y4Al	3.23	3.27	3.34	98.8	96.7
HP1Y4Al_4	2.79	3.22	3.30	86.6	84.5
HP0.7YS	2.91	3.30	--------	88.2	-------

***** Note that values of greater than 100% theoretical density can be observed because the theoretical density calculation is based on the rule of mixtures. The calculation is done using the Y_2O_3 and Al_2O_3 as grain boundary phases, whereas in reality, other phases, which can be denser, form during sintering. Mass losses due to evaporation of SiC/Al_2O_3 and not the dense Y_2O_3, will also increase the measured density of the material.

4.1.2 Gas Pressure Sintering (GPS)

Various gas pressure sintering cycles were used. Heating rates, intermediate holding time and starting gas pressure were varied as described in Table 4.2, in order to optimise the gas pressure sintering of the different composition materials. The final sintering temperature was 1925^{o}C and gas pressure 80 bar.

Table 4.2 Description of the gas pressure sintering cycles

Cycle	Mean heating rate (K/min)	Holding time at 1875^{o}C	Starting gas pressure (bar)
A	5	30	1
B	10	30	1
C	5	60	1
D	10	60	2

The aim of the gas pressure sintering was to minimise the mass loss and maximise the density. The mass loss and density results of cycles A and B are shown in Table 4.3 and those of cycles C and D are shown in Table 4.4.

Cycle A was successful in densifying the four lower Y_2O_3-content compositions, but could not successfully densify the highest yttria content material (GP4Y1Al). Cycle B was an experiment to test whether the gas pressure sintering would be as successful if the heating rate was increased. The faster heating rate in B resulted in higher mass loss in all the materials and had no effect on the densification of the three lowest Y_2O_3-content materials. The faster heating rate in B resulted in lower density of the GP4Y2Al material.

Usually, the organic additives in the samples to be gas pressure sintered were removed under Ar at 1200^{o}C. One composition (GP1Y4Al) was burnt out additionally in air at 450^{o}C. For this composition the difference in temperature and conditions for removal of organic additives did not appear to influence the densification, since dense materials were obtained in both

cases. To summarise: all of the compositions except the two highest Yttria-content compositions (GP4Y1Al and GP4Y2Al) could be densified using Cycles A and B.

Table 4.3 Results of first set of gas pressure sintering experiments

Materi-al	Mass loss (%)		ρ (g/cm^3)		Open porosity (%)		$\rho_{theory1}$ (g/cm^3)	$\rho_{theory2}$ (g/cm^3)
	Cycle A	Cycle B	Cycle A	Cycle. B	Cycle A	Cycle B		
1Y4Al (Burn out at 450°C)	-----	3.4	-----	3.25	-----	0.45	3.27	3.34
1Y4Al (Burn out at 1200°C)	3.3	3.3	3.26	3.26	0.24	0.42	3.27	3.34
3Y5Al	2.2	2.4	3.30	3.30	0	0	3.28	3.35
1Y1Al	1.6	2.0	3.32	3.32	0	0.001	3.29	3.36
4Y2Al	1.1	1.7	3.27	3.07	0	0.01	3.29	3.37
4Y1Al	0.9	-----	3.05	-----	1.01	-----	3.30	3.37

Open porosity less than 0.2% is connected only with the roughness of the surface and not with the sintering.

Cycles C and D were an attempt to improve the densification in the two highest Y_2O_3-content materials, GP4Y1Al and GP4Y2Al (these results are seen in Table 4.4). GP4Y2Al could only be densified to nearly theoretical density, by increasing the intermediate holding time before applying the gas pressure in Cycle C. However, Cycle C could not be accepted as a successful program, because evaporation from the different components in the furnace, condensing on the pyrometer window, resulted in problems of reading of the temperature by the pyrometer. To combat this problem, a program, Cycle D, was adopted where the heating rate, and the gas pressure was increased slightly at an intermediate temperature. This lowered condensation on the window, but there was no improvement in the densification.

As can be seen in Table 4.4, even cycle D did not produce dense materials. This could be because of the faster heating rate used in Cycle D, which, as was seen in the comparison between cycles A and B, the higher Y_2O_3-containing materials were not densified with a faster heating rate. The densification of the GP4Y2Al achieved in cycle C, which could not be reproduced with cycle D, could also be because the sintering temperature in cycle C was actually higher than what the pyrometer read.

Table 4.4 Results of sintering cycles C and D for the high Y-content samples

Compo-sition	Mass loss (%)		ρ (g/cm^3)		Open porosity (%)		$\rho_{theory1}$ (g/cm^3)	$\rho_{theory2}$ g/cm^3)
	Cycle C	Cycle D	Cycle C	Cycle D	Cycle C	Cycle D		
4Y2Al	2.1	2.3	3.32	3.02	0.01	1.06	3.29	3.37
4Y1Al	0.68	1.3	3.02	2.94	0.3	8.16	3.30	3.37

Since cycle A was the most successful in sintering the four main (the four lower Y_2O_3-content) compositions, the gas pressure sintering samples which were studied further in this work were those produced by Cycle A (summarised in Table 4.5).

Table 4.5 Comparison of the mass loss and the densities of samples after different runs with the same cycle ("slower cycle": Cycle A)

Compo-sition	Mass loss (%)		ρ (g/cm^3)		Open porosity (%)		$\rho_{theory1}$ (g/cm^3)	$\rho_{theory2}$ (g/cm^3)
	RUN 1 A1	RUN 2 A2	RUN 1 A1	RUN 2 A2	RUN 1 A1	RUN 2 A2		
1Y4Al	3.4	3.3	3.26	3.26	0.25	0.24	3.27	3.34
3Y5Al	2.4	3.0	3.30	3.30	0.00	0.00	3.28	3.35
1Y1Al	1.9	2.4	3.32	3.31	0.02	0.01	3.29	3.36
4Y2Al	1.6		3.03		0.10		3.29	3.37

4.1.3 Post sintering heat treatments

Post-sintering heat treatments of HP-W materials were carried out at 1900^{o}C and 1700^{o}C. Experiments were not considered to be successful

since mass losses were very high (between 4 and 8 mass-%). A summary of the results is given in Table 4.6 below.

Table 4.6 Summary of heat treatment of HP-W materials

Material	Mass loss (mass-%)	Density (g/cm^3)	Density (%)	Relative grain growth (estimate)
HP-W 3Y5Al HT 1900°C, 2 hours	8	3.20		**
HP-W 1Y1Al HT 1900°C, 2 hours	8	3.17		*
HP-W 4Y2Al HT 1900°C, 2 hours	4	3.23		*
HP-W 1Y1Al HT 1700°C, 2 hours	6	3.12		***

Post-sintering heat treatments were carried out on both the hot pressed and gas pressure sintered materials. These heat treatments were done under similar conditions to gas pressure sintering at 1925°C and 1975°C. The differences were that the heating rate was slightly higher (average 10K/minute), and there was no holding time to increase the gas pressure at an intermediate temperature.

Table 4.7 gives the mass losses of the materials during the post-sintering heat treatments. In this table it is observed that the highest mass loss was observed in the HP1Y4Al material heat treated at 1975°C (4.2 mass-% loss). The general trend in mass loss was for a decrease in mass loss with decrease in alumina content, and mass loss was observed to be higher in the hot pressed than in the gas pressure sintered materials.

All the materials were close to theoretical density before heat treatment (less than 1% porosity), except for the GP4Y2Al material. In Table 4.8 one sees that an overall increase in density of these materials was observed during heat treatment, except for a decrease in density for the GP4Y2Al material. In section 5.1 these results are discussed.

Table 4.7 Mass losses of materials during post sintering heat treatments

Materials	Mass loss (%)			
	HT2 (1.5 h 1925°C)	HT3 (5 h 1925°C)	HT4 (8 h 1925°C)	HT5 (5h 1975°C)
HP1Y4Al	2.83	3.46	3.36	4.23
HP3Y5Al	1.96	2.37	2.37	2.00
HP1Y1Al	1.89	1.65	1.5	1.95
HP4Y2Al	1.85	1.36	1.47	1.86
HP4Y1Al	---	---	---	-0.13
GP1Y4Al	0.59	1.1	1.39	1.29
GP3Y5Al	-0.31	-0.13	0.08	0.30
GP1Y1Al	-0.27	0.22	0.22	0.10
GP4Y2Al	0.12	0.26	0.31	0.34

Table 4.8 Densities of post-sintering heat treated materials

Material	Density (g/cm^3)			
	HT2 (1.5 h 1925°C)	HT3 (5 h 1925°C)	HT4 (8 h 1925°C)	HT5 (5 h 1975°C)
HP1Y4Al	3.27	3.27	3.26	3.25
HP3Y5Al	3.30	3.30	3.35	3.39
HP1Y1Al	3.33	3.34	3.35	3.31
HP4Y2Al	3.33	3.33	3.33	3.29
GP1Y4Al	3.27	3.26	3.26	3.26
GP3Y5Al	3.31	3.30	3.31	3.30
GP1Y1Al	3.33	3.32	3.33	3.31
GP4Y2Al	3.05	3.03	3.00	2.90

4.2 Qualitative and Quantitative Phase Analysis (X-Ray diffraction) and X-ray Fluorescence (XRF)

The XRD diffraction pattern were analysed qualitatively using the JCPDS database. The amounts of the found phases were then quantified using the Rietveld method. Rietveld refinement calculations were performed on scanned XRD data of the different LPSSiC materials produced. The quantitative phase content of the materials, obtained from these calculations, is shown in Table 4.9, 4.10, 4.11 and 4.12.

Table 4.9 Summary of qualitative and quantitative SiC polytype content determination of the HP-W materials

Material	**SiC 6H**	**SiC4H**	**SiC15R**	**SiC 3C**
HP3Y5Al-W	69.0±1.3	6.6±0.8	13.4±1.1	4.0±0.9
HP1Y1Al-W	68.5±1.4	7.5±1.0	13.0±1.1	5.3±1.0
HP4Y2Al-W	71.5±1.5	6.4±1.0	12.1±1.2	4.4±1.1

Table 4.10 Grain boundary phase content in HP-W materials

Material	**$Y_3Al_5O_{12}$ (YAG)**	$Y_{4.67}(SiO_4)_3O$ (Apatite)
HP3Y5Al-W	7.0±0.2	
HP1Y1Al-W	5.7±0.2	
HP4Y2Al-W	4.0±0.2	1.6±0.2

The calculations done based on XRD –scans of the solid pieces of sintered materials gave an apparent texture of especially the YAG phase in gas pressure sintered materials. Because of the isotropic pressure application in gas pressure sintering, there should be no observed preferred orientation of YAG crystals. The apparent observed texture in YAG must have been due to larger crystals of YAG in the solid material. Such large crystals caused the relative intensities of the peaks to be falsely distributed.

Table 4.11 Summary of qualitative and quantitative SiC polytype content determination of the LPSSiC materials

No.	Material	SiC 6H	SiC4H	SiC15R	SiC 3C
1	HP1Y4Al	62.9±3.3	4.0±1.5	5.9±1.8	17.5±2.6
2	HT2HP1Y4Al	64.1±1.2	10.4±1.6	16.2±1.4	
3	HT3HP1Y4Al	65.5±1.5	10.2±1.1	10.5±1.1	4.5±1.0
4	HT4HP1Y4Al	-----	-----	-----	-----
5	HT5HP1Y4Al	47.5±1.5	27.4±1.5	18.7±1.7	
6	GP1Y4Al	69.9±1.4	6.8±0.9	11.8±1.1	2.8±1.1
7	HT2GP1Y4Al	69.0±1.7	9.7±1.3	9.5±1.3	5.0±1.0
8	HT3GP1Y4Al	66.0±1.7	13.7±1.3	12.6±1.41	1.0±1.0
9	HT4GP1Y4Al	-----	-----	-----	-----
10	HT5GP1Y4Al	41.3±1.0	33.7±1.1	20.6±1.2	
11	HP3Y5Al	71.7±1.7	9.7±1.2	9.2±1.1	2.8±1.2
12	HT2HP3Y5Al	64.8±1.5	8.7±1.1	12.8±1.4	4.5±1.2
13	HT3HP3Y5Al	67.8±1.2	7.8±0.9	11.8±1.1	2.2±0.8
14	HT4HP3Y5Al	-----	-----	-----	-----
15	HT5HP3Y5Al	57.1±1.7	15.5±1.9	14.2±2.2	
16	GP3Y5Al	67.6±1.6	10.1±1.1	8.0±1.1	5.2±1.2
17	HT2GP3Y5Al	64.5±1.1	9.2±1.3	16.3±1.4	0.00
18	HT3GP3Y5Al	65.0±1.9	10.9±1.2	10.7±1.3	4.0±1.4
19	HT4GP3Y5Al	-----	-----	-----	-----
20	HT5GP3Y5Al	58.1±1.2	18.2±1.1	16.2±1.4	
21	HP1Y1Al	68.9±0.8	7.6±0.8	13.4±1.0	
23	HT2HP1Y1Al	43.2±11.7	12.4±3.9	42.1±16.2	
24	HT3HP1Y1Al	64.8±1.7	15.3±1.4	9.7±1.3	1.5±1.1
25	HT4HP1Y1Al	59.6±1.7	15.1±1.7	12.9±1.9	1.4±0.2
26	HT5HP1Y1Al	56.2±2.0	16.4±1.6	17.2±2.0	
27	GP1Y1Al	64.8±1.3	11.6±1.2	9.2±1.2	4.9±1.0
28	HT2GP1Y1Al	68.5±1.2	9.6±0.8	10.8±1.0	2.4±0.8
29	HT3GP1Y1Al	67.0±1.2	9.0±0.8	12.8±1.0	1.6±0.9
30	HT4GP1Y1Al	59.1±1.3	15.5±1.2	16.3±1.4	
31	HT5GP1Y1Al	-----	-----	-----	-----
32	HP4Y2Al	68.6±1.4	9.3±1.1	10.4±1.1	2.4±1.2
33	HT2HP4Y2Al	70.9±1.2	14.3±1.4	8.5±1.4	
34	HT3HP4Y2Al	62.7±1.0	12.5±0.8	11.5±0.9	1.5±0.4
35	HT4HP4Y2Al	-----	-----	-----	-----
36	HT5HP4Y2Al	51.4±1.7	25.4±1.5	14.2±1.8	
37	GP4Y2Al	65.0±1.0	11.1±0.9	11.4±1.0	2.2±0.8
38	HT2GP4Y2Al	59.6±1.1	12.7±0.8	13.7±0.2	1.5±0.8
39	HT3GP4Y2Al	54.5±1.1	16.9±1.2	17.6±1.4	
40	HT4GP4Y2Al	59.3±1.6	15.9±1.3	17.5±1.8	
41	HT5GP4Y2Al	58.9±1.6	19.6±1.4	14.3±1.8	
42	HP4Y1Al	67.3±1.6	11.6±1.2	8.4±1.2	3.5±1.3

----- indicates not calculated

Table 4.12 Grain boundary phase content of LPSSiC materials

No.	**Material**	**Y_2SiO_5**	**β-$Y_2Si_2O_7$**	**YAG**	**$Y_4Al_2O_9$**	**$YAlO_3$**	**Al_2O_3**
1	HP1Y4Al		3.3±0.4				6.3±1.0
2	HT2HP1Y4Al			6.2±0.3			3.1±0.7
3	HT3HP1Y4Al			5.7±0.2			3.7±0.5
4	HT4HP1Y4Al*			6.3±0.6			
5	HT5HP1Y4Al			6.5±0.4			
6	GP1Y4Al			6.0±0.2			2.7±0.5
7	HT2GP1Y4Al			6.8±0.3			
8	HT3GP1Y4Al			6.7±0.3			
9	HT4GP1Y4Al			4.56±0.6			
10	HT5GP1Y4Al			4.5±0.2			
11	HP3Y5Al			6.5±0.2			
12	HT2HP3Y5Al			9.3±0.3			
13	HT3HP3Y5Al			10.1±0.2		0.4±0.1	
14	HT4HP3Y5Al			0.00			
15	HT5HP3Y5Al			13.2±1.8			
16	GP3Y5Al			9.1±0.2			
17	HT2GP3Y5Al			10.0±0.3			
18	HT3GP3Y5Al			9.4±0.3			
19	HT4GP3Y5Al			0.00			
20	HT5GP3Y5Al			7.6±0.5			
21	HP1Y1Al		4.5±0.3	5.6±0.2			
23	HT2HP1Y1Al			1.4±0.4	0.9±0.3		
24	HT3HP1Y1Al					8.6±0.3	
25	HT4HP1Y1Al			3.3±0.3		7.7±0.4	
26	HT5HP1Y1Al					10.1±1.2	
27	GP1Y1Al			5.7±0.2	4.0±0.2		
28	HT2GP1Y1Al			2.9±0.8	1.0±0.1	4.8±0.2	
29	HT3GP1Y1Al			1.4±0.1		8.2±0.3	
30	HT4GP1Y1Al			2.1±0.2		7.0±0.3	
31	HT5GP1Y1Al						
32	HP4Y2Al	5.3±0.3		3.9±0.2			
33	HT2HP4Y2Al				6.3±0.2		
34	HT3HP4Y2Al				6.2±0.2	5.6±0.2	
35	HT4HP4Y2Al						
36	HT5HP4Y2Al			0.7±1.4	5.5±0.3	2.7±0.3	
37	GP4Y2Al			0.2±0.1	8.1±0.2	2.0±0.2	
38	HT2GP4Y2Al				9.3±0.2	3.2±0.2	
39	HT3GP4Y2Al				5.7±0.3	5.3±0.3	
40	HT4GP4Y2Al				6.1±0.3	1.1±0.3	
41	HT5GP4Y2Al				7.3±0.3		
42	HP4Y1Al	9.2±0.4					

*Traces of Si were found in all the gas pressure sintered and heat treated materials, (as a small bump at 2theta = 28.45^o), but quantified in particular by Rietveld analysis in these heat treated materials:

In HT4HP1Y4Al: 0.6 ± 0.2, in HT4GP1Y4Al: 0.5± 0.3, in HT4HP3Y5Al: 0.7±0.2, and in the HT4GP3Y5Al: 0.4±0.2 (similar to what reference 97 observed during pressureless sintering at 2050^{o}C).

XRF scans were done on the hot pressed and gas pressure sintered materials to determine whether there were any impurities in the LPSSiC materials. The results, in Table 4.13, showed that there were traces of Fe in nearly all the materials, as shown in the XRF spectra of the GP3Y5Al material in Figure 4.1.

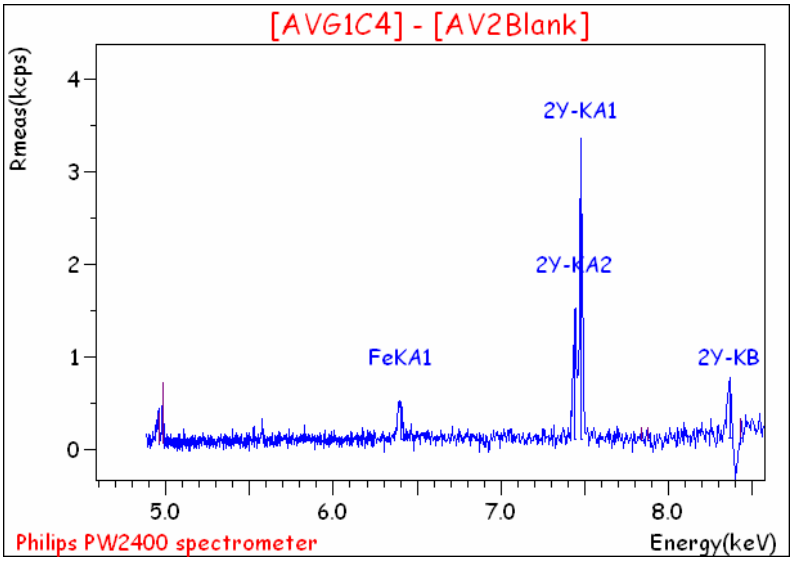


Figure 4.1 Part of XRF scan to show the presence of traces of Fe impurity in the GP3Y5Al material

The presence of traces of iron and calcium is not surprising, since the UF15SiC powder manufacturers, H.C. Starck, state that impurities Al (up to 0.03 mass-%), Ca (up to 0.01 mass-%) and Fe (up to 0.05 mass-%) are present in the powder[69].

Table 4.13 Results of XRF scans

Material	Impurities found (trace amounts)
HP1Y4Al	None
HP3Y5Al	Fe, Gd
HP1Y1Al	None
HP4Y2Al	None
HP4Y1Al	None
GP1Y4Al	Ni
GP3Y5Al	None
GP1Y1Al	None
GP4Y2Al	Ni
SSiC	Ca, P

4.3 Quantitative microstructural analysis (FESEM)

The microstructures of the LPSSiC materials produced in this research were studied using the Field Emission Scanning Electron Microscope (FESEM) and using the "IMAGANALYSIS" software program for quantitative analysis. The microstructural parameters were calculated from thirty FESEM micrographs, analyzing between approximately 3600 and 7200 grains per material. The SiC mean grain size was calculated from area distribution, assuming equivalent circular diameter. A summary of these results are shown in Table 4.14. Examples of some FESEM micrographs are given in Figures 4.2 – 4.9. More FESEM micrographs of the hot pressed, gas pressure sintered and post-sintering heat treated materials can be seen in Appendix C.

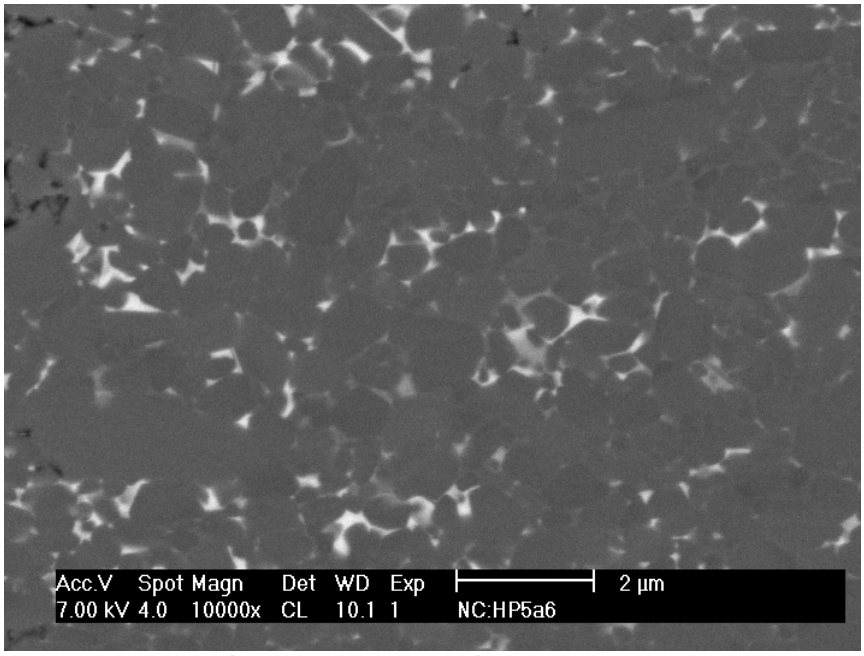


Figure 4.2 FESEM micrograph of HP1Y4Al material

Table 4.14 Summary of the results of the microstructural image analysis calculations (MFP = mean free path)

Material	SiC mean Grain size (μm)	ECD std-dev*	SiC MFP (μm)	Mean Triple junc-tion size (μm)	Grain bound-ary MFP (μm)	SiC Cont-ent (%)	SiC Contig-uity (%)	Grain bound-ary conten t (%)
HP1Y4Al	1.32	0.562	1.34	0.40	0.14	94.03	70.49	5.97
HT2HP1Y4Al	2.6	1.26	2.25	0.75	0.21	94.42	66.06	5.58
HT3HP1Y4Al	2.84	1.52	3.19	0.85	0.25	95.14	75.74	4.86
HT4HP1Y4Al	4.17	2.39	3.81	0.79	0.29	93.68	71.23	6.32
GP1Y4Al	3.24	1.8	2.76	0.52	0.23	93.82	71.52	6.18
HT2GP1Y4Al	3.02	1.91	2.88	0.68	0.23	93.71	73.60	6.29
HT3GP1Y4Al	4.21	2.21	3.92	1.03	0.27	94.39	71.70	5.61
HT4GP1Y4Al	5.50	3.88	4.46	1.64	0.35	94.19	69.97	5.81
HP3Y5Al	1.01	0.42	0.90	0.65	0.18	89.41	59.77	10.59
HT2HP3Y5Al	1.94	1.02	1.71	0.78	0.25	90.27	63.44	9.73
HT3HP3Y5Al	2.73	1.92	2.47	0.87	0.32	89.62	66.71	10.38
HT4HP3Y5Al	2.86	1.69	2.73	0.89	0.35	90.31	69.45	9.69
GP3Y5Al	2.13	0.85	2.26	0.64	0.26	90.38	70.38	9.62
HT2GP3Y5Al	2.68	1.26	2.55	0.86	0.32	90.51	69.63	9.49
HT3GP3Y5Al	2.74	1.64	2.54	0.93	0.32	89.53	67.40	10.47
HT4GP3Y5Al	2.76	1.53	2.65	1.65	0.35	90.04	68.56	9.96
HP1Y1Al	0.93	0.39	0.75	0.52	0.14	88.60	57.19	11.40
HT2HP1Y1Al	1.93	1.08	2.12	0.56	0.22	91.39	71.35	8.61
HT3HP1Y1Al	2.62	1.70	2.59	0.71	0.31	90.43	69.80	9.57
GP1Y1Al	1.90	0.94	1.93	0.60	0.23	89.21	68.53	10.79
HT2GP1Y1Al	2.32	1.19	2.27	0.81	0.25	91.14	69.16	8.86
HT3GP1Y1Al	3.10	2.50	2.75	0.81	0.33	90.68	69.84	9.32
HP4Y2Al	0.92	0.39	0.74	0.54	0.15	87.66	56.67	12.34
HT2HP4Y2Al	2.18	1.44	1.77	0.86	0.31	85.67	59.47	14.33
HP4Y1Al	0.92	0.39	0.81	0.59	0.17	86.99	56.19	13.01

* Note that the standard deviations get higher as the grain size distribution broadens

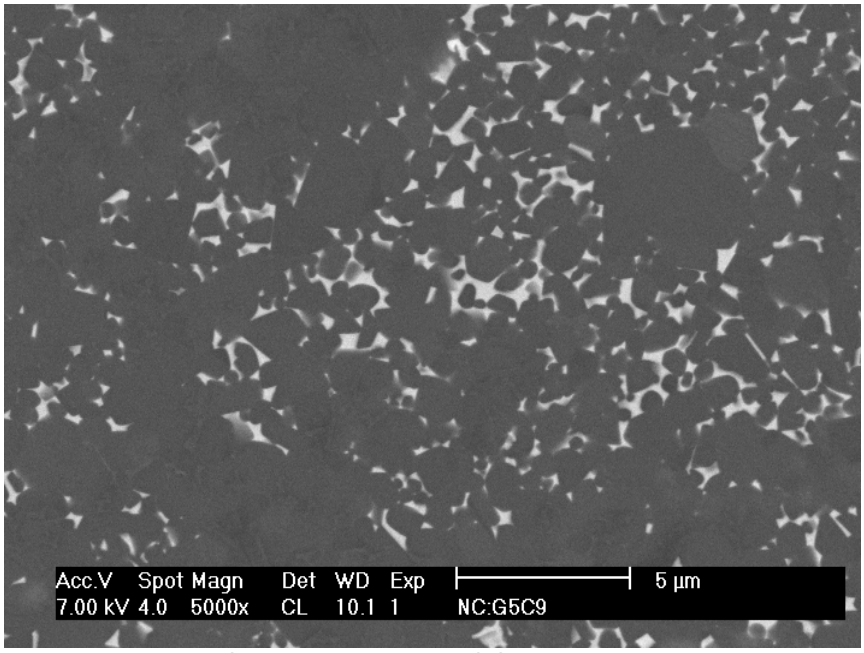


Figure 4.3 FESEM micrograph of GP1Y4Al material

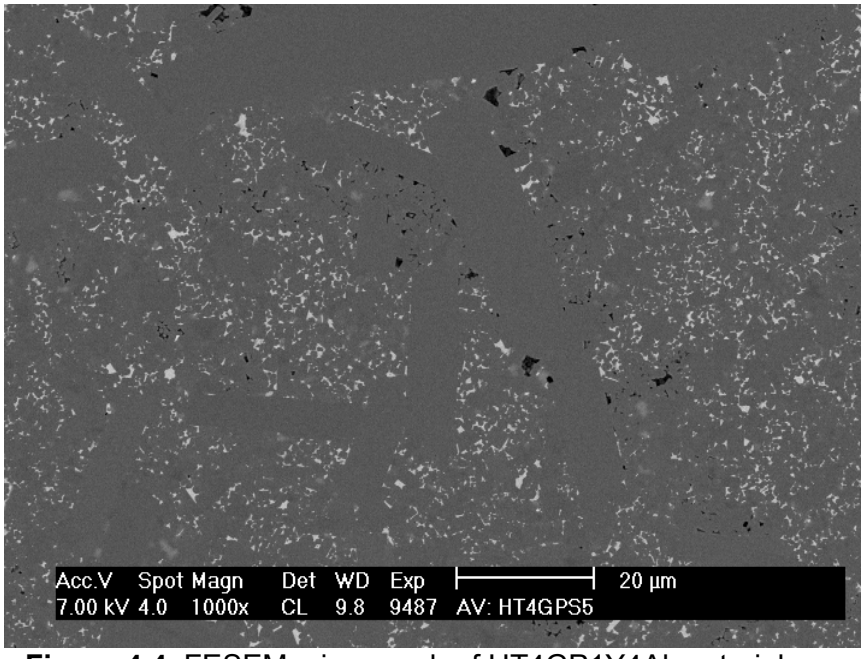


Figure 4.4 FESEM micrograph of HT4GP1Y4Al material

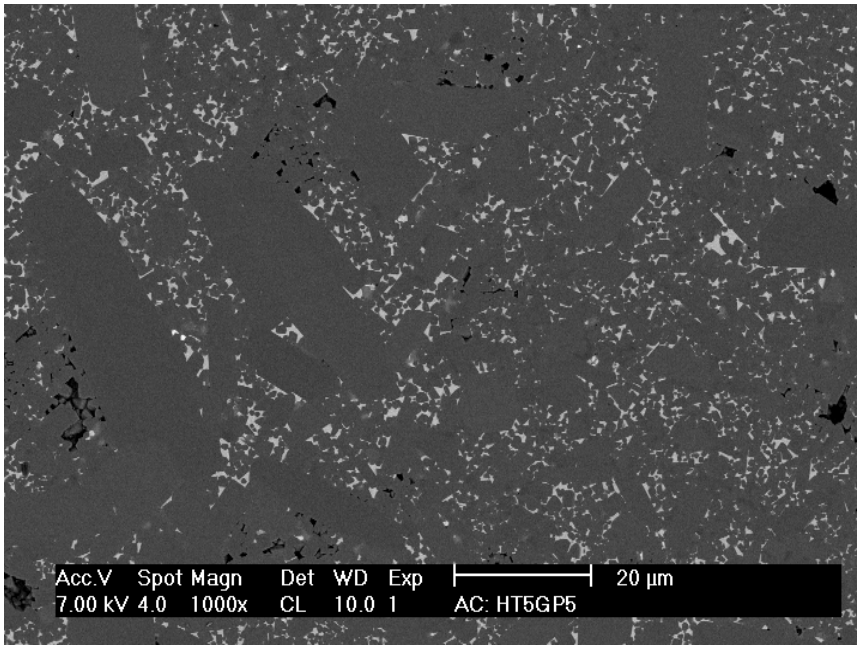


Figure 4.5 FESEM micrograph of HT5GP1Y4Al material

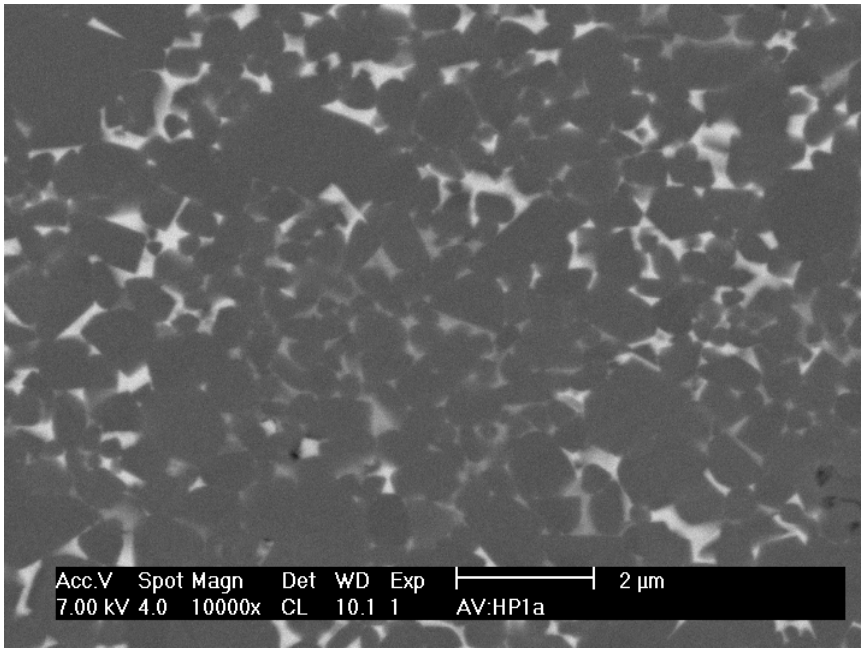


Figure 4.6 FESEM micrograph of HP3Y5Al material

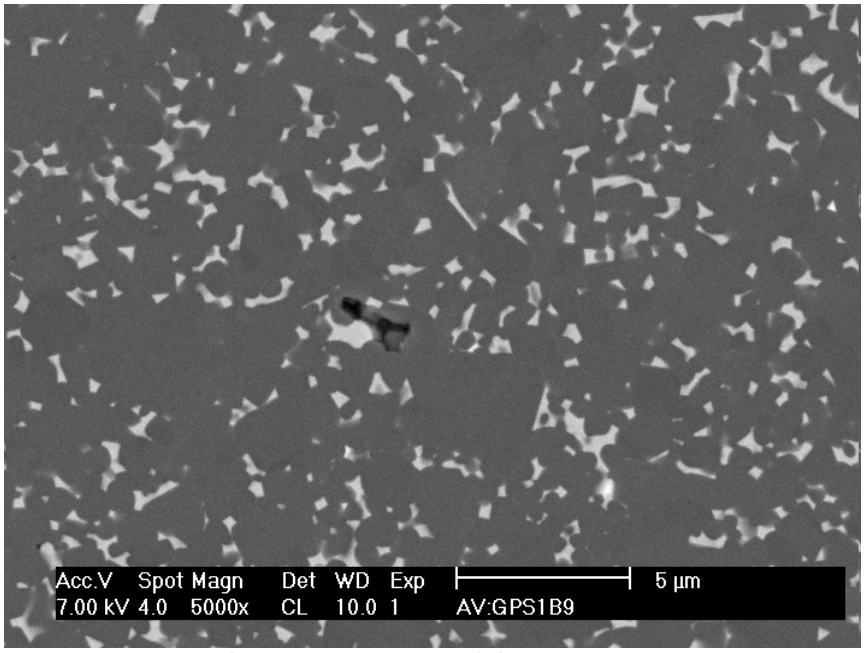


Figure 4.7 FESEM micrograph of GP3Y5Al material

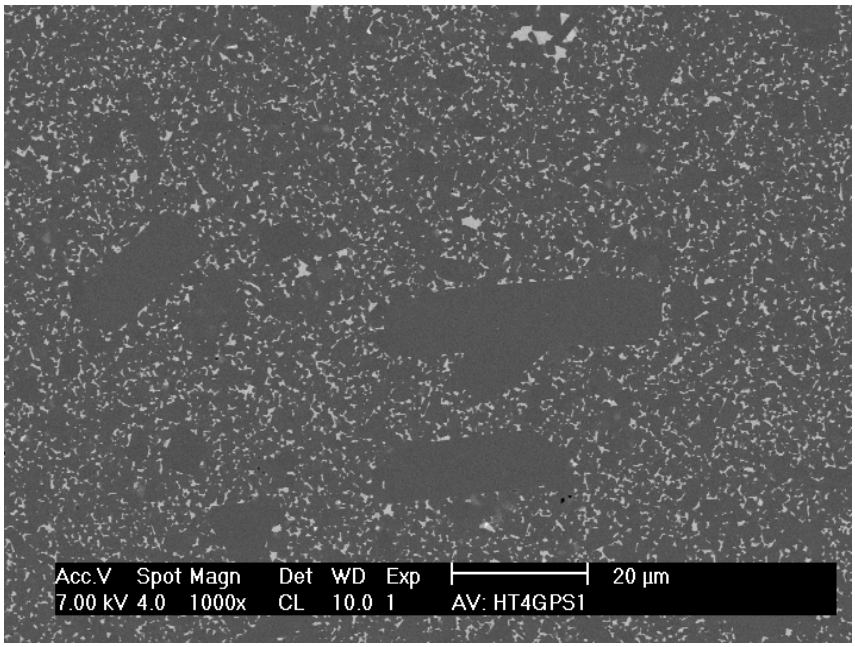


Figure 4.8 FESEM micrograph of HT4GP3Y5Al material

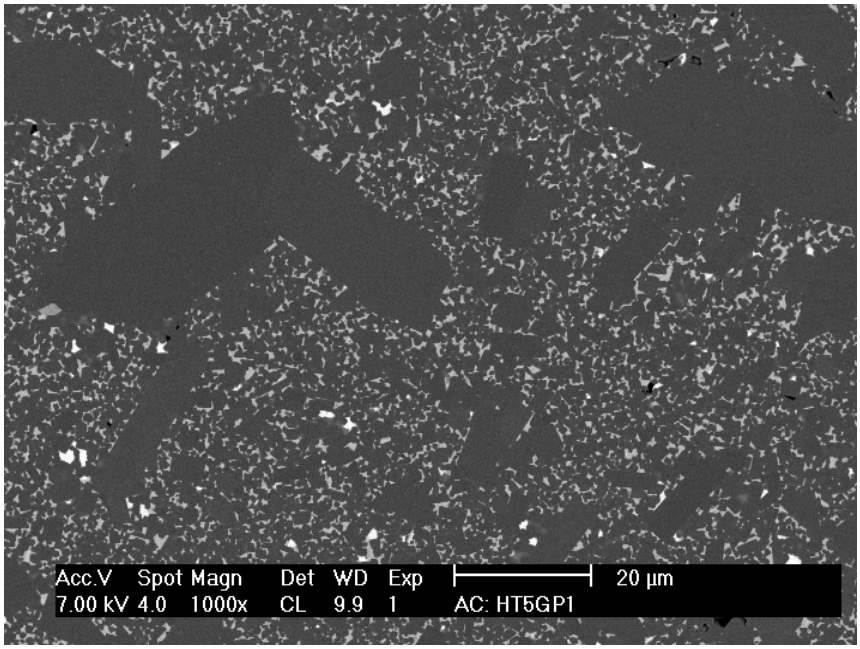


Figure 4.9 FESEM micrograph of HT5GP3Y5Al material

As is seen in the figures in Figures 4.10 and 4.11, the grain size distributions in the hot pressed and gas pressure sintered materials are unimodal. The grain size distributions were narrowest for the HP materials, and slightly broader in the GPS materials. The grain size distributions broadened with each consequent heat treatment, and were consistently higher for the higher alumina content materials**.** The grain size distribution in the heat treated materials broadened with subsequent heat treatments (as seen in Figures 5.24 and 5.25). Additional silicon carbide grain size distribution curves can be seen in Appendix D.

Figure 4.12 shows how the mean free path of the grain boundary material increases after each heat treatment.

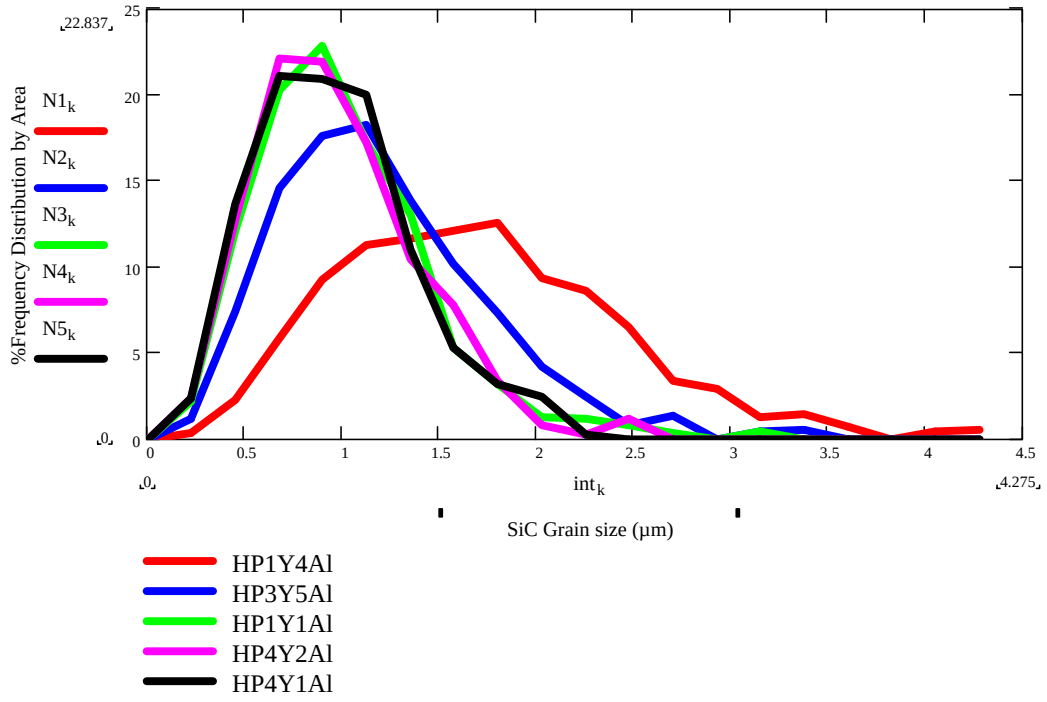


Figure 4.10 Silicon carbide grain size distributions for the HP materials

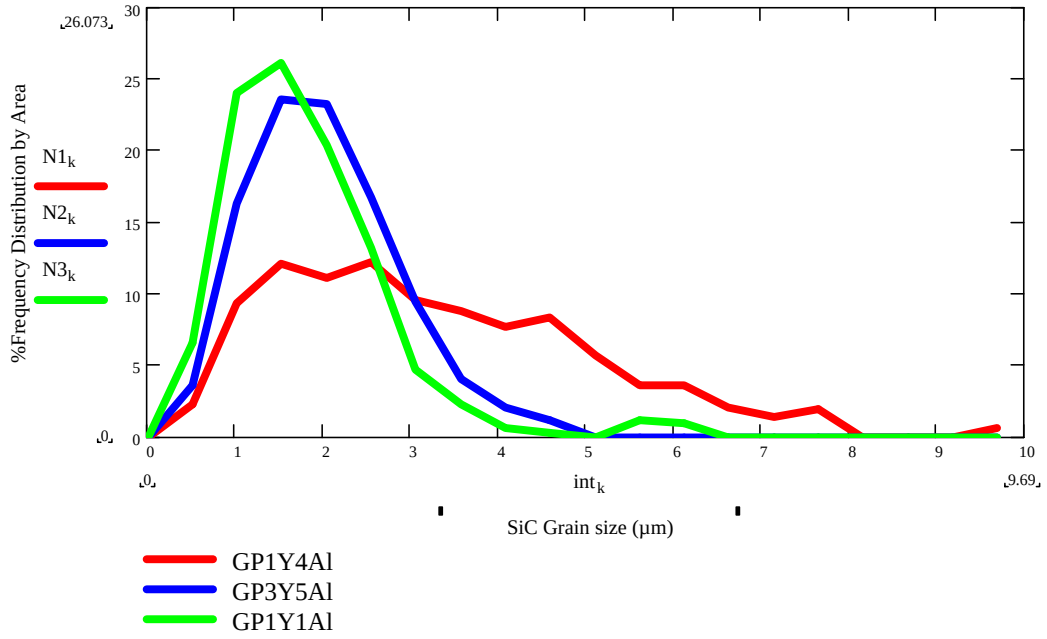


Figure 4.11 Silicon carbide grain size distributions for the GPS materials

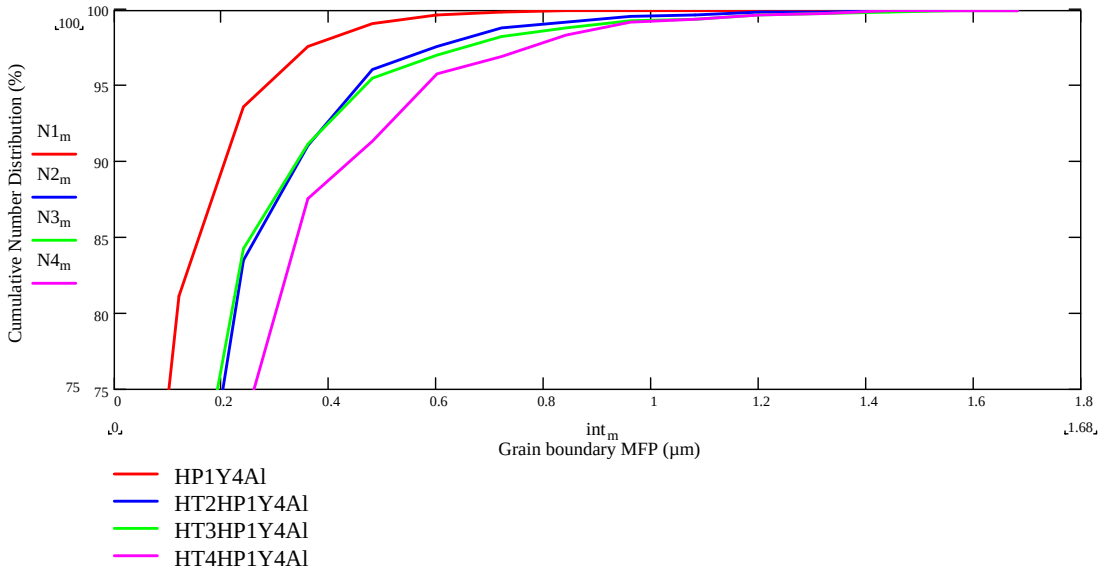


Figure 4.12 Grain boundary mean free path number distribution during HT for the HP1Y4Al material

4.4 Mechanical Properties of the Materials

Elastic modulus, hardness, indentation fracture toughness and strength of the selected materials were measured and the results are shown in this section.

4.4.1 Elastic modulus, Vicker's hardness and indentation toughness

Hardness was measured on two different pieces of equipment, both Vickers hardness indenters. The first is labelled V1 and the second, V2. A summary of these hardness and fracture toughness results is given in Table 4.15. The experimental data of these two series of measurements are slightly different, therefore a series of scaling measurements were done on one piece of equipment (V3) and these will be used to compare the hardness and fracture toughness of the different materials. These measurement results are shown in Table 4.16.

No significant difference in hardness in the HP-W and HP materials was observed for the different compositions, as can be seen in Table 4.15.

Table 4.15 Summary of elastic modulus, Vicker's hardness and fracture toughness of the LPSSiC materials

Material	HV10 (GPa)	K_{1C} ($MPam^{1/2}$)	E (GPa)	Equipment used
HP3Y5Al-W	21.8±1.3	4.3±0.4	---	V1
HP1Y1Al-W	21.2±0.8	3.3±0.2	---	V1
HP4Y2Al-W	21.7±0.7	3.9±0.2	---	V1
HP1Y4Al	20.4±0.3	3.7±0.4	384	V2
HP3Y5Al	20.1±0.5	3.7±0.1	396	V2
HP1Y1Al	20.9±0.6	3.5±0.3	398	V2
HP4Y2Al	20.7±0.9	3.5±.0.2	403	V2
HP4Y1Al	20.3±0.4	3.4±0.4	406	V2
GP1Y4Al	25.6±1.9	3.5±.0.5	427	V2
GP3Y5Al	26.2±0.7	3.2±0.1	435	V2
GP1Y1Al	25.1±1.7	3.5±.0.3	437	V2
GP4Y2Al	11.00*	*	311	V2
HT2 HP1Y4Al	24.8±0.5	4.0±0.4	426	V2
HT3 HP1Y4Al	24.2±1.0	4.3±0.5	436	V2
HT4 HP1Y4Al	21.9±0.6	4.5±0.3	419	V1
HT5 HP1Y4Al	19.7 ±0.9	5.1±0.7	----	V2
HT2HP3Y5Al	23.4±0.4	3.5±0.2	438	V2
HT3HP3Y5Al	23.3±0.5	3.6±.0.1	433	V2
HT4HP3Y5Al	21.8±1.3	3.8±0.3	438	V1
HT5HP3Y5Al	18.6±0.6	5.6±1.3	----	V2
HT2HP1Y1Al	24.9±0.3	3.6±0.4	---	V2
HT3HP1Y1Al	24.3±0.7	3.7±0.6	----	V2
HT4HP1Y1Al	----	----	424	---
HT5HP1Y1Al*	--------	-------	----	V2
HT2HP4Y2Al	21.6±0.3	3.8±0.3	428	V2
HT3HP4Y2Al	23.1±1.6	3.3±0.3	411	V2
HT4HP4Y2Al	----	----	410	---
HT5HP4Y2Al	18.6±1.2	4.3±0.2	----	V2
HT2GP1Y4Al	25.39±0.35	4.1±0.2	428	V2
HT3GP1Y4Al	24.4±1.2	4.7±0.7	428	V2
HT4GP1Y4Al	22.2±1.2	4.9±0.7	419	V1
HT5GP1Y4Al	17.9±1.7	5.2±0.7		V2
HT2GP3Y5Al	24.4±0.4	3.7±0.2	435	V2
HT3GP3Y5Al	23.5±1.3	3.9±0.4	431	V2
HT4GP3Y5Al	22.3±0.5	4.3±0.5	428	V1
HT5GP3Y5Al	19.6±1.4	4.9±0.7	----	V2
HT2GP1Y1Al	24.0±.0.9	3.4±0.2	----	V2
HT3GP1Y1Al	22.6±0.7	3.8±0.6	----	V2
HT4GP1Y1Al	----	----	434	--
HT5GP1Y1Al	19.9±1.1	4.8±0.6	----	V2
HT2GP4Y2Al	----	----	303	---
HT3GP4Y2Al	----	----	297	---
HT4GP4Y2Al	----	----	287	---
HT5P4Y2Al*	8.41±2.42*	*	----	V2

* not measurable

Table 4.16 shows the results of the hardness and fracture toughness measurements which were made on the different Vickers' hardness indenters. The trends observed (as described below) are the same for the different equipment measurements. There is an increase in hardness after the first heat treatment, and then it does not change very much during subsequent heat treatments. There is a slight decrease in hardness during the heat treatment at higher temperature (HT5, which is a heat treatment for 5 hours at 1975^{o}C).

The fracture toughness of the materials do not appear to change after the 1.5 hour (HT2) and 5 hour (HT3) heat treatment at 1925^{o}C. After the 8 hour heat treatment at 1925^{o}C, there appears to be a significant increase in the fracture toughness. A more significant increase in fracture toughness is however observed when the sintered materials are heat treated at a higher temperature (1975^{o}C) for 5 hours. These observations are confirmed by the results of the measurements done on equipment V3, shown in Table 4.16.

Table 4.16 Hardness and fracture toughness measurements made on V3 for comparison purposes

Material	**HV10 (GPa) Previous**	**HV10 (GPa) V3**	**K_{1C} (MPam$^{1/2}$) Previous**	**K_{1C} (MPam$^{1/2}$) V3**
HP3Y5Al	20.07±0.48(V2)	20.40±0.81	3.7±0.1(V2)	3.8±0.3
HT2HP3Y5Al	23.35±0.43(V1)	23.43±1.00	3.5±0.2(V2)	3.5±.0.2
HT3 HP3Y5Al	23.34±0.46(V2)	22.57±0.86	3.6±0.1(V2)	3.7±0.5
HT4 HP3Y5Al	21.84±1.29(V1)	25.46±0.64	3.8±0.3(V1)	4.1±0.2
HT5 HP3Y5Al	18.55±0.56(V2)	24.22±2.6	6.2±1.5(V2)	5.2±0.7
HP1Y4Al	20.40±0.33(V2)	20.23±0.28	3.7±.4(V2)	3.5±0.3
HT2HP1Y4Al	24.80±0.45(V2)	24.43±0.30	4.0±.4(V2)	3.7±0.1
HT4 HP1Y4Al	21.92±0.61(V1)	21.00±0.18	4.5±0.3(V1)	5.1±0.3
HT5 HP1Y4Al	19.73±0.86(V2)	20.50±0.52	4.5±.0.2(V2)	5.1±0.6
GP1Y1Al	25.09±1.68(V2)	23.04±0.23	3.5±.0.3(V2)	3.5±0.2

Hardness measurements were made on the HP3Y5Al also at elevated temperatures. The results are given in Figure 4.13.

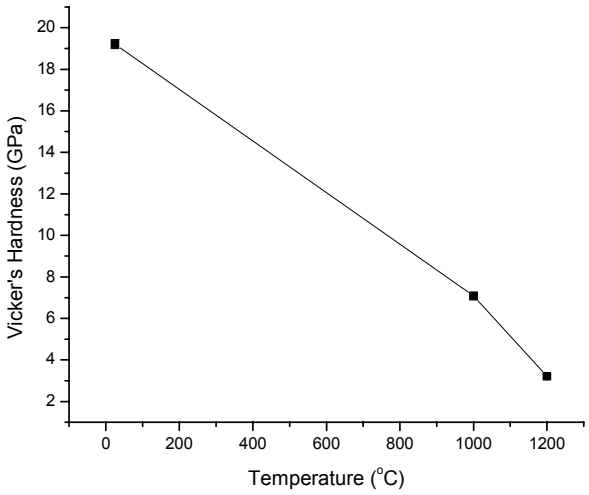


Figure 4.13 Results of the high temperature hardness measurement carried out on the HP3Y5Al material

The surface of the sample, perpendicular to the direction of hot pressing, as well as a cross-section (parallel to the direction of hot pressing) of selected HP-W samples was polished and tested for fracture toughness and crack resistance. When the indentation cracks on the cross-section were studied, the crack lengths in the direction perpendicular and parallel to the direction of hot pressing were measured.

A plot of the sum of crack lengths versus the load applied in a Vicker's indentation test, given as Figure 4.14, was done to determine the crack resistance of the materials. The crack resistance values were derived from the slope of this curve, and are summarized in Table 4.17.

The HP3Y5Al-W and the HP1Y1Al-W material showed very similar crack resistance. The HP4Y2Al-W showed very high standard deviation in terms of crack length (given in Figure 4.14).

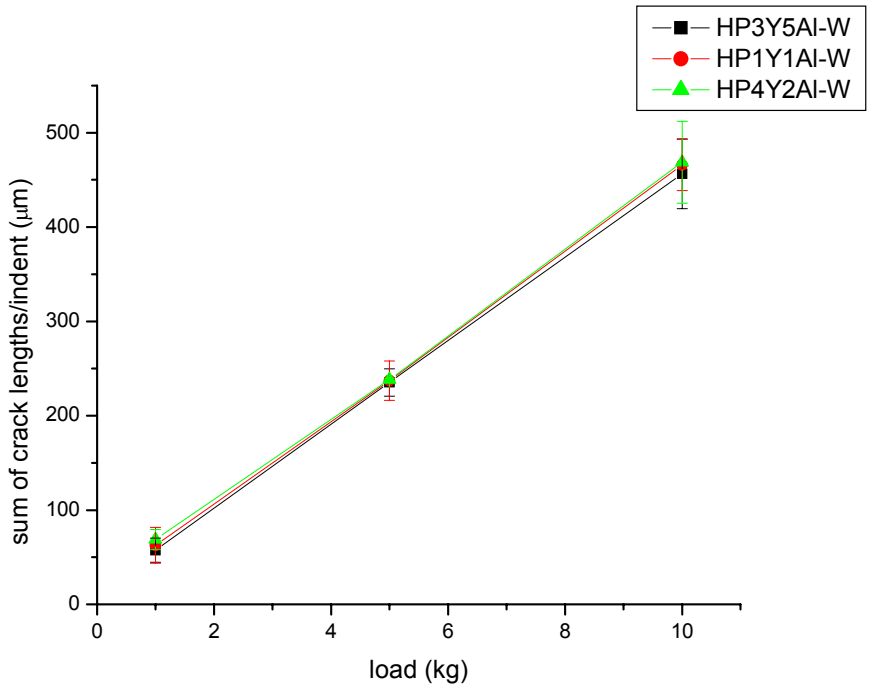


Figure 4.14 Graph showing the crack resistance of HP-W materials (on cross-section of material)

Table 4.17 Fracture toughness and crack resistance results

Material	HP3Y5Al-W	HP1Y1Al-W	HP4Y2Al-W
K_{1c} – surface (MPa.m$^{1/2}$)	3.6 ± 0.2	3.4 ± 0.3	3.9 ± 0.3
K_{1c} – cross-section - perpendicular (MPa.m$^{1/2}$)	4.1 ± 0.5	3.1 ± 0.3	3.6 ± 0.2
K_{1c} – cross-section - parallel (MPa.m$^{1/2}$)	4.5 ± 0.3	3.7 ± 0.2	4.3 ± 0.4
Crack resistance – perpendicular (kg/μm)	0.044	0.043	0.040
Crack resistance - parallel (kg/μm)	0.049	0.052	0.051

This crack resistance measurement was done on a cross-section (perpendicular to the direction of hot pressing) and a surface tangential to the direction of hot pressing. Some anisotropy was observed in the hot–pressed HP-W materials.

The number of intergranular fractures, transgranular fractures and crack bridging was counted along a determined length of cracks under FESEM for selected LPSSiC materials. The roughness of the cracks was also determined and these results are shown in Table 4.18.

Table 4.18 Results of analysis of crack under FESEM

Material	Indentation fracture toughness ($MPam^{1/2}$)	Roughness	Ratio intergranular to transgranular fracture/ length (μm^{-1})	No. of Crack bridges/ length (μm^{-1})
HP3Y5Al*	3.7±0.1	1.35±0.08	0.086±0.005	0.23±0.04
HP1Y4Al*	3.7±0.4	1.40±0.03	0.20±0.01	0.21±0.06
GP3Y5Al	3.2±0.1	1.31±0.05	0.11±0.12	0.12±0.04
GP1Y4Al	3.5±0.5	1.31±0.03	0.058±0.02	0.10±0.03
HT3G1Y4Al	4.7±0.7	1.37±0.05	0.15±0.07	0.16±0.06

*only two cracks analysed in these samples, therefore results are not as reliable

4.4.2 Four-point bending strength and fractographical study of the materials

Four-point bending strength tests were done on the hot pressed and gas pressure sintered materials only and the results are shown in Table 4.19. After testing selected fractured surfaces were studied to determine the origin of failure.

The cause of failure in one of the samples of the HP3Y5Al material was found to be an isolated area of iron impurities (area of length 10 microns), shown in Figures 4.15 and 4.16. This was only observed in one sample and therefore it is believed that this impurity does not come from the processing technology, but is more likely to be from the original SiC powder used (where Fe is reported to be an impurity maximum 0.05% (mass fraction)[69].

Table 4.19 Four point bending strength results of HP and GPS materials

Composition	HP (not tempered)Strength, σ_{4B} (MPa)	HP (tempered1250°C) Strength σ_{4B} (MPa)	GPS (tempered1250°C) Strength σ_{4B} (MPa)
1Y:4Al	473±120[1)]	519±58	526±39
3Y:5Al	657±50	607± 78	456±58
1Y:1Al	609±55	545± 46	366±32
4Y:2Al	518±105[2)]	564± 47	-------
4Y:1Al	486±41	533±39	-------

Note that the high standard deviations observed for 1) and 2) marked in Table 4.19 is because of one very low strength value measured for one sample.

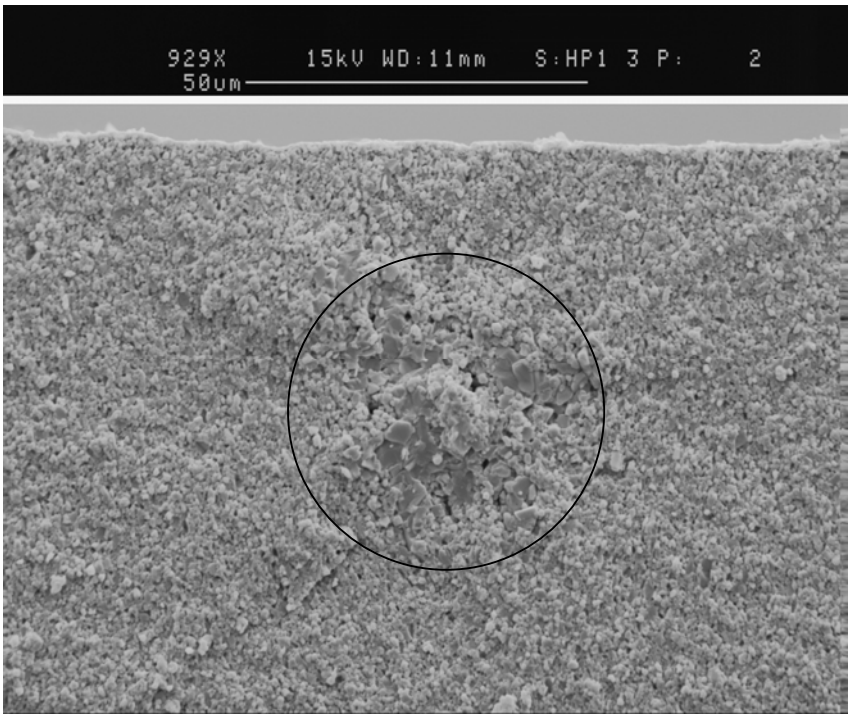


Figure 4.15 SEM micrograph showing origin of failure in HP3Y5Al material. EDS analysis of the marked larger grains, confirmed the presence of iron impurities (in dark region in circle)

In the two materials where the Y_2O_3 content was higher HP4Y1Al and HP4Y2Al, large Y-rich agglomerates (most likely Y_2O_3) (50-200 micron), were observed to be the cause of failure in only two of the samples of this composition.

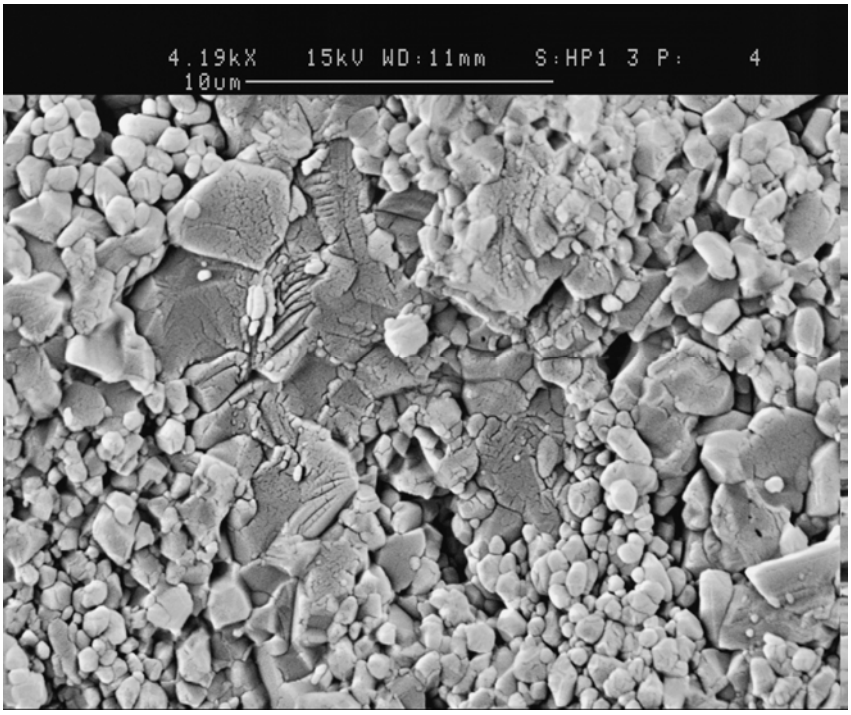


Figure 4.16 SEM micrograph showing the origin in failure (iron impurities), as shown in Figure 4.15, at a higher magnification

4.5 Electrical Properties

A dc measurement measures only the average material property, whereas ac measurements, or Impedance Spectroscopy, allow one to separate the contributions of different phases in the material. Ac electrical properties of the LPSSiC ceramics were measured. For comparison purposes, in addition to the LPSSIC materials sintered with Y_2O_3 and Al_2O_3, one solid-state sintered SiC (SSiC) sintered with boron and carbon additives, and one LPSSIC material sintered with Y_2O_3 and SiO_2 as the sintering additives, were also measured. Electrical measurements were made at

different temperatures ranging from liquid nitrogen temperature (-196^{o}C) up to 330^{o}C.

4.5.1 Ac conductivity behaviour of the different materials at a fixed temperature

Plots of the log of the ac conductivity as a function of the log of angular frequency is given in Figure 4.17 (measured at 200^{o}C) and Figure 4.18 (measured at 330^{o}C).

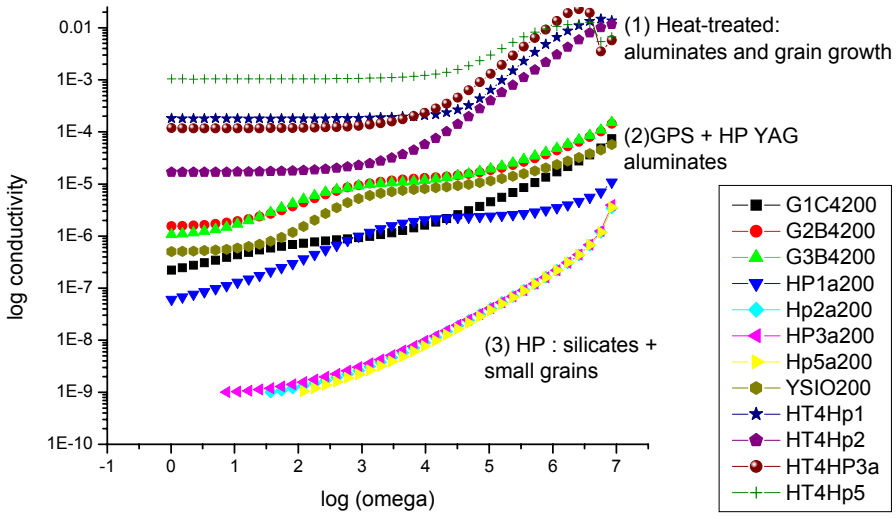


Figure 4.17 Graph of the log of electrical conductivity as a function of the log of angular frequency at 200^{o}C. In the labels 1 = 3Y5Al, 2 = 4Y2Al, 3= 1Y1Al, 4 = 4Y1Al, 5 = 1Y4Al

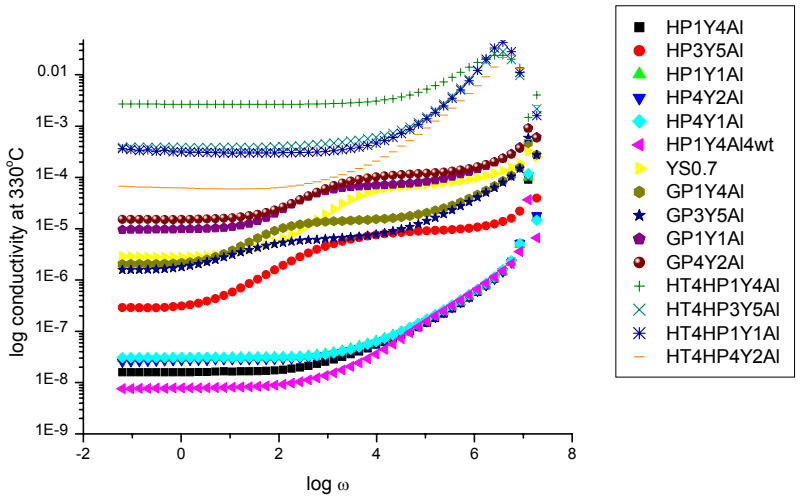


Figure 4.18 Graph of the log of electrical conductivity as a function of the log of angular frequency at 330°C

As indicated in Figure 4.17, there are three groups of materials with similar dc conductivities and electrical behaviour. The shapes of the curves indicate that the bottom group and top group correspond to two-phase percolative systems. The middle group corresponds to a three-phase system. Relationships between these log conductivity results and the microstructures of the different LPSSiC materials, will be discussed in detail in section 5.3.

Similar log conductivity curves were obtained when measuring with the Solartron equipment. The plot of log conductivity vs log ω can be seen in Figure E1 in Appendix E.

4.5.2 Cole-Cole plots of the LPSSiC materials

At 200°C, all of the hot pressed materials, with the exception of HP3Y5Al, only show one arc in the impedance spectra (Cole-Cole plots). Recall from the experimental section that the Cole-Cole plot is a plot of the negative imaginary impedance, -Z'', versus the real impedance, Z'. An

example of this one arc observation in the hot pressed materials is given in Figure 4.19.

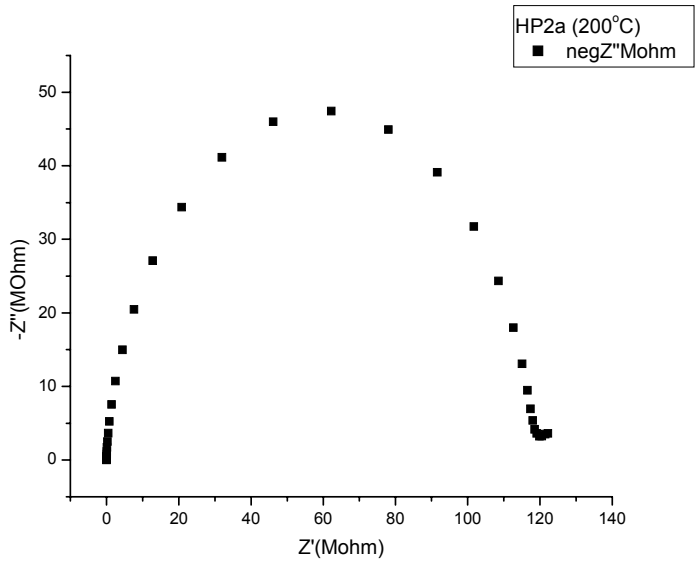


Figure 4.19 Cole- Cole plot of HP4Y2AI material at 200°C

Figure 4.20 shows that HP3Y5AI does show a small “bump” as indication of a second phase. The gas pressure sintered materials, for example the GP3Y5AI material shown in Figure 4.21, on the other hand show very clearly distinguished two arcs, for all the compositions at 200°C.

The single arc observed in the HP materials is a low conductivity, low frequency phase, which corresponds to the lower conductivity part of the heat treated log conductivity plots.

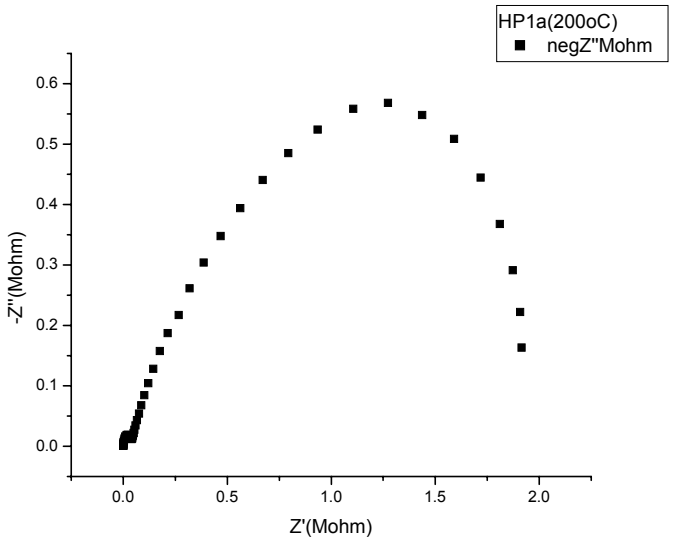


Figure 4.20 Cole –Cole plot of HP3Y5Al material at 200^{o}C

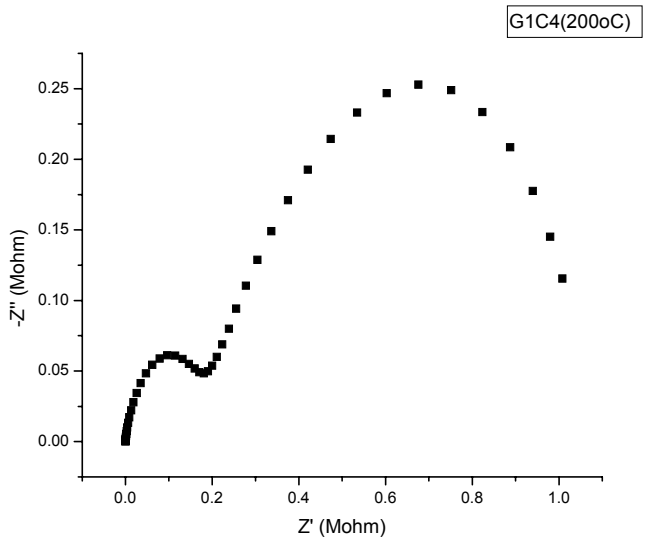


Figure 4.21 Cole-Cole plot of GP3Y5Al material at 200^{o}C

In the heat treat treated HP materials, at 200^{o}C, only one arc was observed. Another observation, which was only seen in the heat treated HP materials Cole-Cole plots, was the “curling in” tail-effect on the extreme right (low frequency) end. This was more pronounced in the three more conducting materials (HT4HP1Y4Al, HT4HP3Y5Al and HT4HP1Y1Al) and

at higher temperature. This can be illustrated by comparing Figure 4.22, which is the Cole-Cole plot for HT4HP4Y2Al at 330°C and Figure 4.23, the Cole-Cole plot for the same material at 300°C.

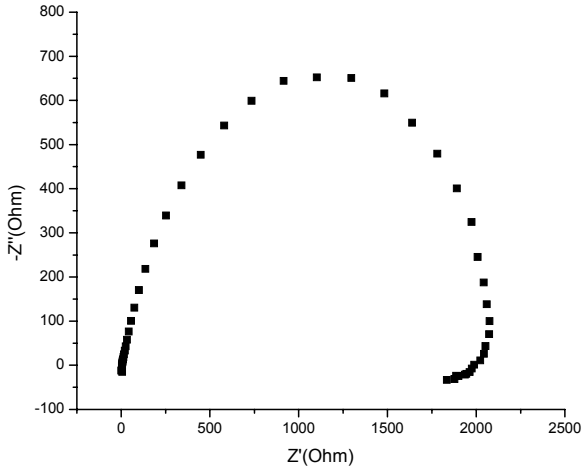


Figure 4.22 Cole-Cole plot of HT4HP4Y2Al at 330°C

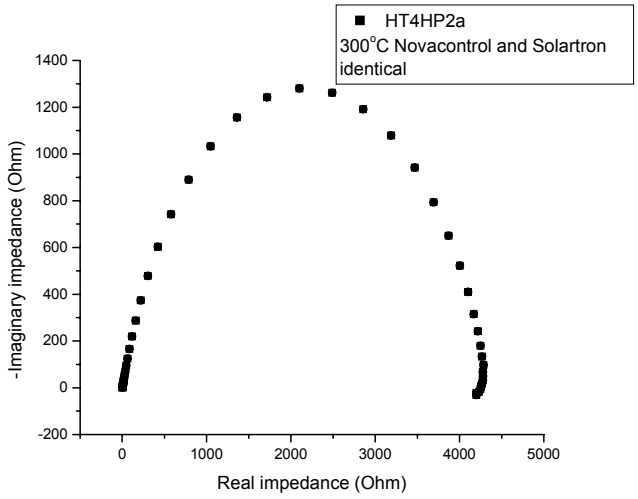


Figure 4.23 Cole-Cole plot of HT4HP4Y2Al at 300°C

Similar observations were made by Macdonald, who attributed this to be due to a complex polarization effect [185].

4.5.3 Temperature dependence of conductivity

According to the Arrhenius-type relationship, given as equation 4.5.2, the temperature dependence of the conductivity was determined by plotting the log of the conductivity vs $1/T^n$, where n is a number, adjusted to give the best fit straight line for a set of experimental data. The conductivity values were obtained from the width of the arcs, as described in the previous section. Tables of the results are given in Appendix E.

A temperature dependence of 1/T, which corresponds to Arrhenius behaviour, typical for semiconductors such as silicon carbide[197], was not observed for samples with conductivities below 10^{-4} at 200°C. The temperature dependence results above log conductivity of 10^{-4} were inconsistent, not giving a straight line when plotting against $1/T^n$, for various values of n over an appreciable range. For the remaining materials, the temperature dependence was found to be $1/T^{1/4}$, which is characteristic of Mott Variable Range Hopping mechanism[191,192]. The linear fit was best observed in the highly insulative HP phases, an example of which is shown in Figure 4.24. This would imply that the contribution of SiC is not observed in any of the impedance plots, except for a possible small contribution for higher conductivity (heat treated HP) samples. This means that most likely only the secondary phase is being observed in these Impedance Spectroscopy results.

From a variable range hopping-fit to the data (such as the one shown in Figure 4.24), an average excitation energy determined was between 0.2 and 0.5 eV (given in Table 4.20). Since the temperature dependence of these phases are not 1/T, this energy should not be referred to as an energy gap, but rather a characteristic temperature/ energy ($E_g = k_B T_g$) of hopping conductivity.

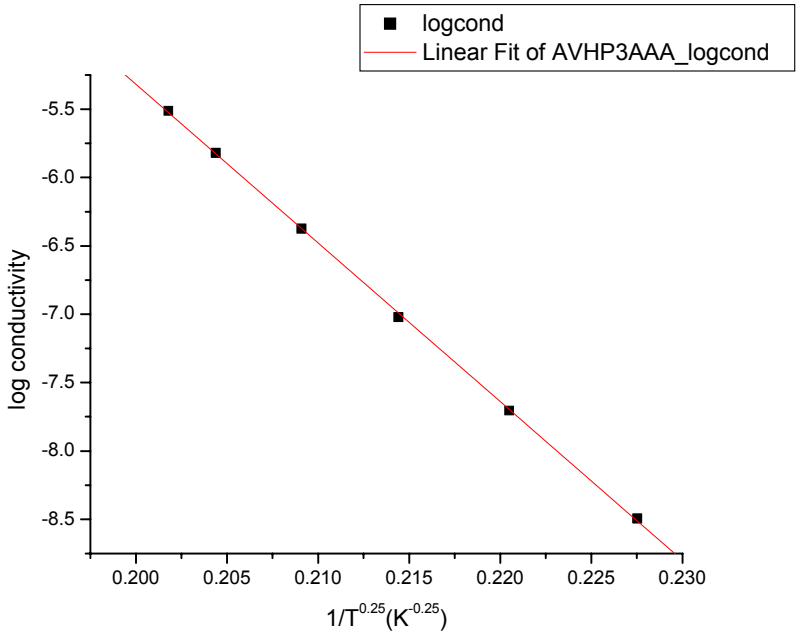


Figure 4.24 Plot of log conductivity vs $1/T^{0.25}$, to show the best fit for the temperature dependence of HP1Y1Al

Table 4.20 Results of excitation energies determined by best-fit to temperature dependence

Material	Best fit for temperature dependence	Excitation energy (eV) 1st arc	Excitation energy (eV) 2nd arc	Conductivity band (Figure 4.5.2)
HP1Y4Al_4	Variable range hopping	0.582	-----	Bottom
HP1Y4Al	Variable range hopping	0.441	-----	bottom
HP1Y1Al	Variable range hopping	0.408	-----	Bottom
HP4Y2Al	Variable range hopping	0.423	-----	Bottom
HP3Y5Al	Variable range hopping	0.138	0.176	Middle
GP3Y5Al	Variable range hopping	0.205	0.249	Middle
GP1Y4Al	Variable range hopping	0.233	0.261	Middle
HP0.7YS	Variable range hopping	0.267	0.286	Middle
GP1Y1Al	Variable range hopping	0.193	0.227	Middle
GP4Y2Al	Variable range hopping	0.205	0.223	Middle
HT4HP4Y2Al	Variable range hopping	0.145	-----	top
HT4HP1Y1Al	Variable range hopping	*	*	Top
HT4HP3Y5Al	Variable range hopping	0.0695	-----	top
HT4HP1Y4Al	Variable range hopping	*	*	Top

* Temperature dependence measurements of these high conductivity samples were inconsistent

4.5.4 Dielectric constant and peak frequency of the different materials

The dc conductivity and peak frequency were determined from the Cole-Cole plots as given in section 4.5.3 above. The peak frequency and corresponding resistance determined from the Cole-Cole plots, were used to calculate the capacitance, according to equation 3.13.

The capacitance and geometrical factor of the samples was then used to calculate the dielectric constant according to equation 3.15. The specific

resistance (resistivity) of the different phases, measured at 200°C, are plotted as a function of material in Figures 4.25 to 4.27.

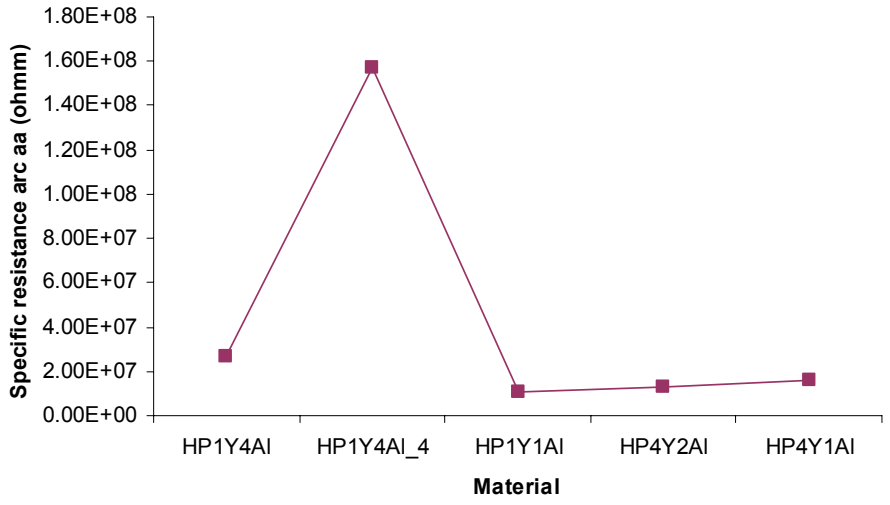


Figure 4.25 Specific resistance (resistivity) results of the only arc observed in the HP materials at 200°C

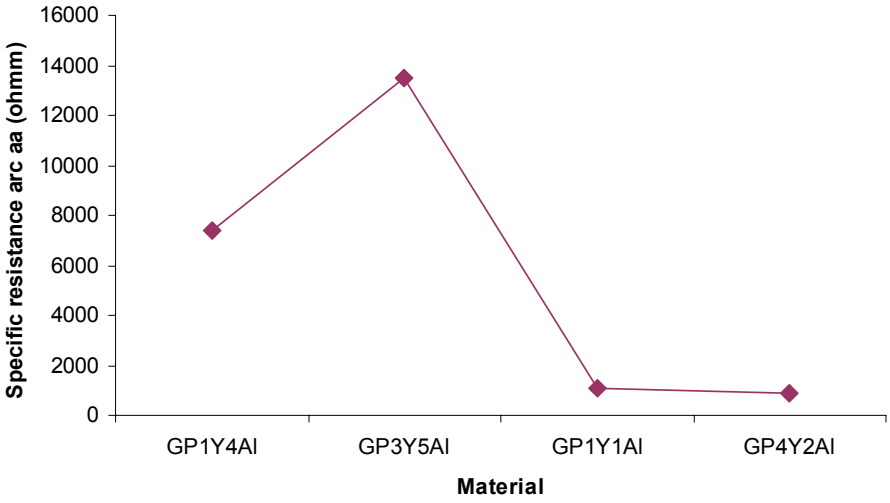


Figure 4.26 Specific resistance (resistivity) results of the 1st, higher frequency arc observed in the GPS materials at 200°C

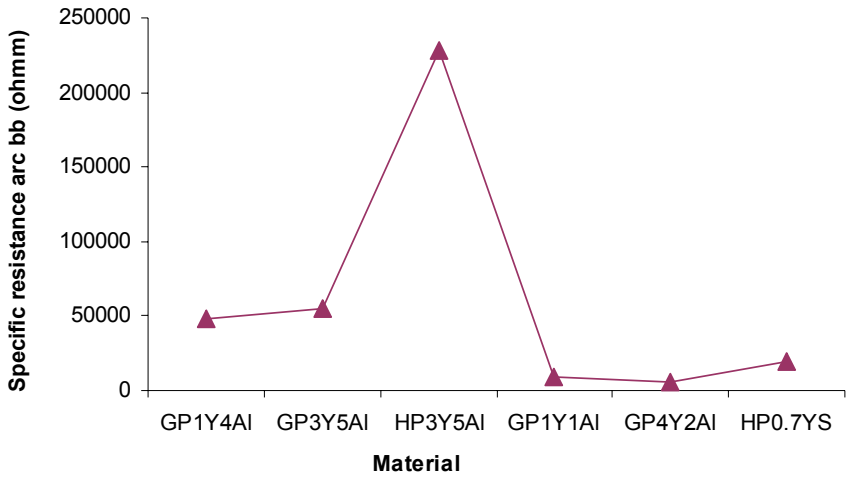


Figure 4.27 Specific resistance (resistivity) results of the 2nd, lower frequency arc observed in the GPS materials at 200°C

The peak frequency results for the different phases are given in Figure 4.28 to 4.30 below.

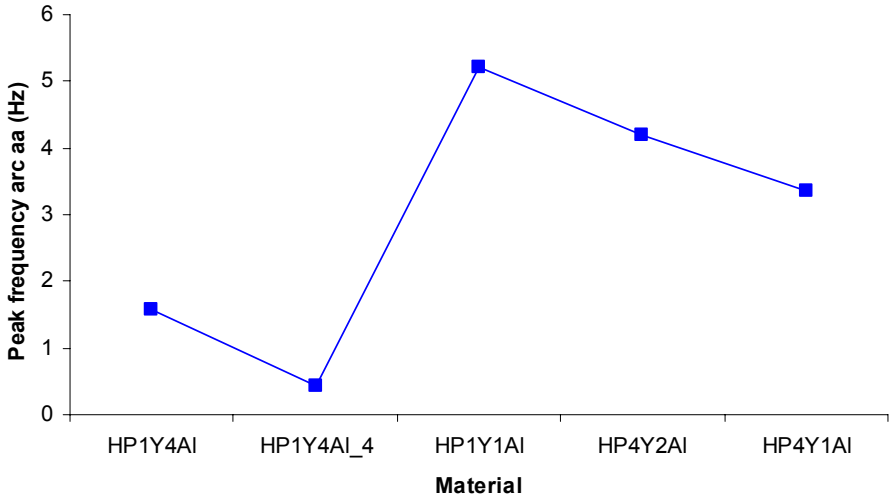


Figure 4.28 Peak frequency of the only arc observed for most of the hot pressed materials at 200°C

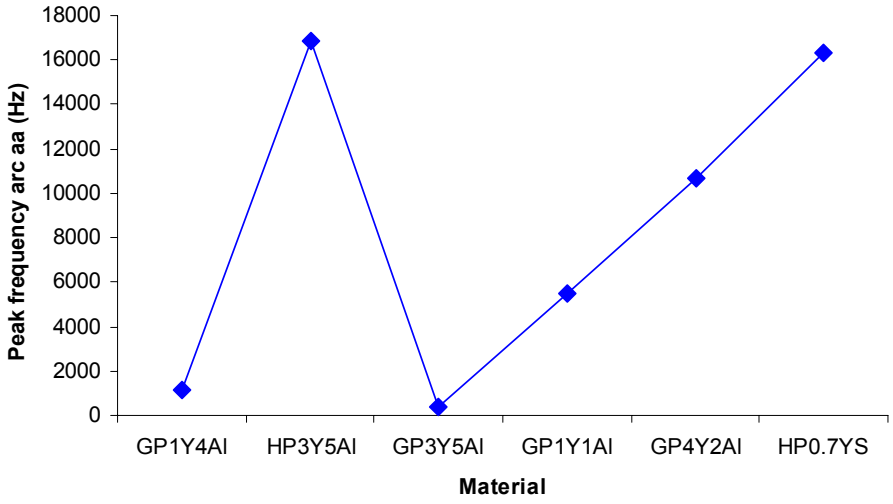


Figure 4.29 Peak frequency of the 1st, higher frequency arc for GPS and HP3Y5Al materials at 200°C

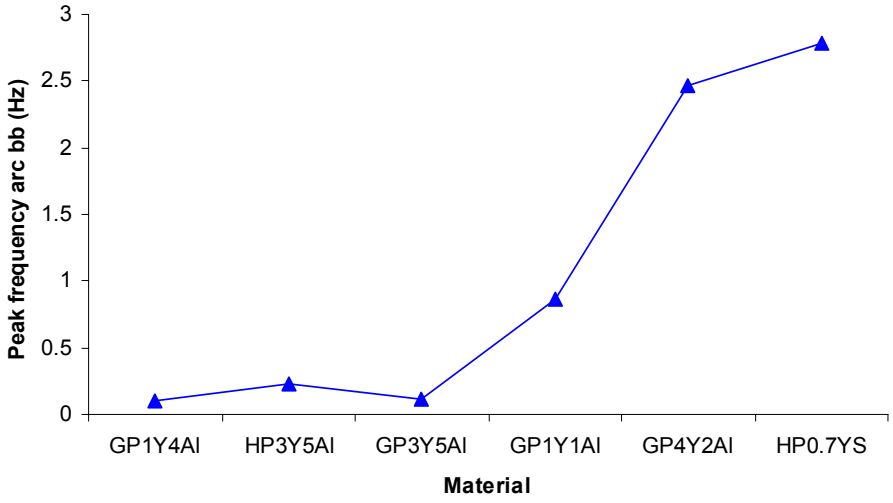


Figure 4.30 Peak frequency for the 2nd, lower frequency arc observed in the GPS and HP3Y5Al and HP0.7YS materials at 200°C

The dielectric constant results at 200°C, as calculated from equation 3.15, are given in Figures 4.31 to 4.33.

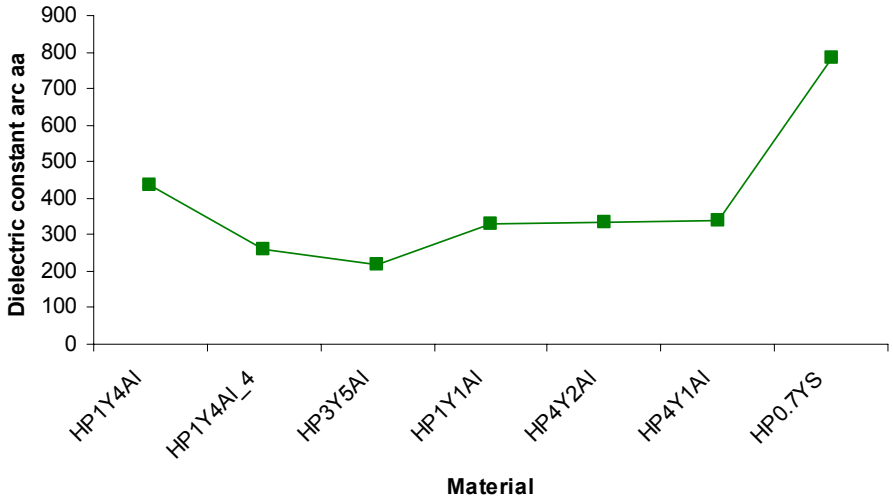


Figure 4.31 Dielectric constant results for the 1st ,higher frequency arc in the HP materials

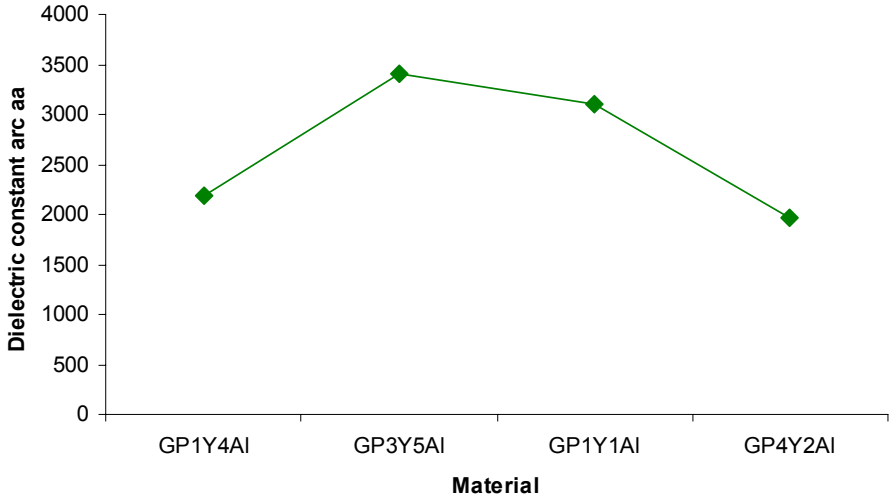


Figure 4.32 Dielectric constant results for the 1st ,higher frequency arc in the GPS materials

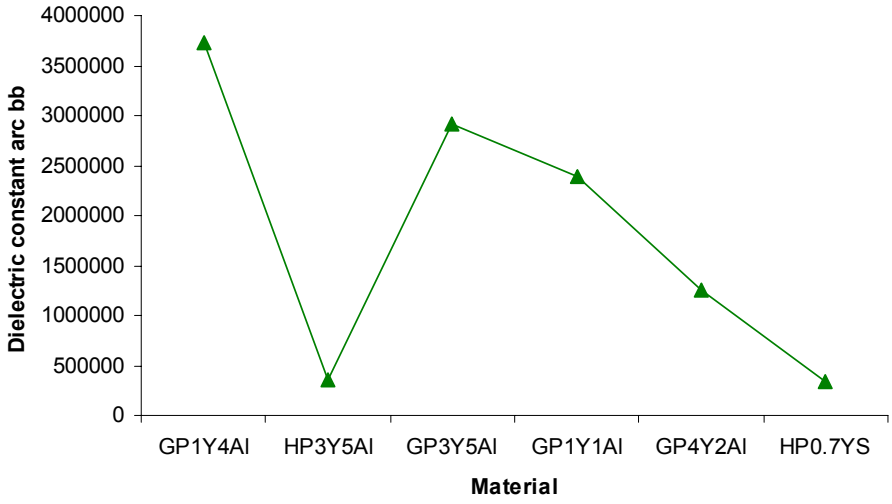


Figure 4.33 Dielectric constant results for the 2nd (lower frequency) arc in the GPS materials

The dielectric constant of the only arc observed in the HP materials is between 200 and 700, which is reasonably high. This would mean that the material could be used as a dielectric, but it would be very lossy at high frequencies. One would have to charge it frequently if one used it as a dc storage capacitor.

Both the phase arcs observed in the GPS materials are much higher than observed in the HP materials. The one arc gives dielectric constant values between 2000 and 3400, and the other, more conducting arc, has a dielectric constant between 1.5 and 4 million! These dielectric constants are very high, however the material could not be used as a storage capacitor because the conductivity is too high.

Comparing the log conductivity plots and the ω_c data, it is observed that the lower characteristic frequencies do correspond to the lower conductivity materials. The wide range for peak frequency values of the highest (or only) frequency phase in the materials, does support the fact that the effect of the silicon carbide is not observed in the log conductivity

and Cole-Cole plots. Very high dielectric constants as observed in Figures 4.31 – 4.33, as are usually observed in poor insulators or high loss dielectrics. Other than these observations, no further meaningful qualitative trends were observed in peak frequency and dielectric constant data. These results, as given in Figures 4.25 to 4.33, will therefore not be further discussed.

dc resistance, dielectric constant and characteristic frequency values calculated for the different materials at room temperature, 100^{o}C, 200^{o}C and 330^{o}C are summarized in Tables in Appendix E.

4.5.5 Ohmic and non-Ohmic behaviour of materials

Some of the materials showed Ohmic and some showed non-Ohmic behaviour. Non-linear response of resistance to changes in activation voltage was used to classify the material as non-Ohmic.

In the 10 mass-% GPS materials, where the electrical behaviour of a second phase was observed, the non-linearity was clearer. This non-linearity was only observed in the second low frequency, higher resistance arc, which is not seen in the HP materials. This is illustrated for the GP3Y5Al material in Figure 4.34. Similar non-Ohmic behaviour was observed when measuring with the Solartron equipment. The result for the Solartron measurements for the GP3Y5Al material can be seen in Figures E2, E3 and E4 in Appendix E. In the HP materials, where only one arc was observed, non- linearity was small, and there was agreement with the dc results. The results were reproducible at different temperatures.

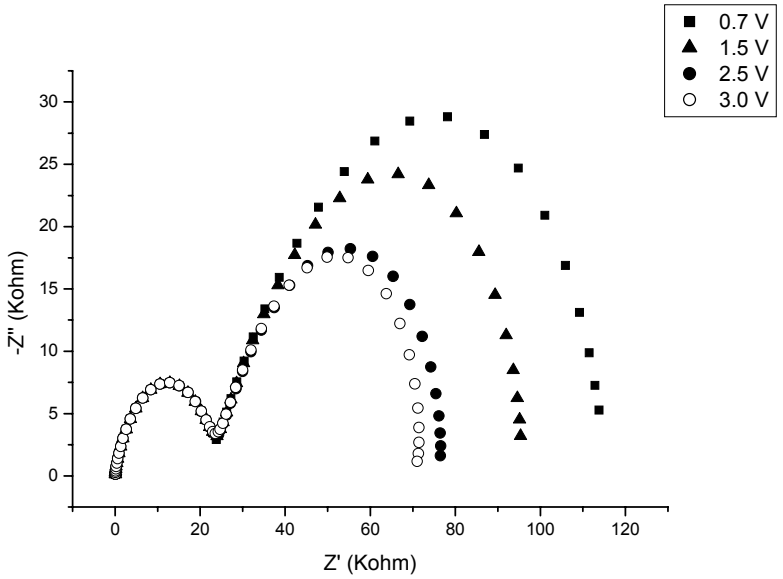


Figure 4.34 Cole-Cole plot of GP3Y5Al material at 330^{o}C showing the non-Ohmic behaviour in the higher resistance phase (Novacontrol)

The results of the SSiC material measured at room temperature were non – linear, but reproducible between the different equipment (Novacontrol and Solartron). The 4 mass-% GPS material with $1Y_2O_3$:$4Al_2O_3$ molar ratio (GP1Y4Al_4) had resistances in the ohm range. Results show that the GP1Y4Al_4 material was also activation voltage sensitive. This non-linearity was therefore observed in the SSiC and all the GPS materials.

4.5.6 Measurement of SSiC, HP0.7YS and GP1Y4Al_4 materials

The 6H single crystal could not be measured because it was too conductive.

The SSiC measured at high temperatures gave nonsensical results, in that measurements made on the same apparatus (Solartron), at the same activation voltage (1.50 V), and at the same temperature, gave inconsistent results. This was perhaps because the SSiC materials was

too conducting for high temperature measurements. As a result of this some measurements on the SSiC were also made at liquid nitrogen temperature (-196^{o}C). Room temperature and liquid nitrogen temperature measurements gave consistent results.

Figure 4.35 below shows the two arcs that were observed for the SSiC materials at room temperature. SSiC measured at room temperature, resulted in two clear arcs, with a little bump appearing at the beginning of the first higher frequency arc. Magnification of this “bump” revealed a third still higher frequency arc. SSiC measured at liquid nitrogen temperature (-196^{o}C) revealed one clear lower frequency arc and a small higher frequency“ bump” at the beginning of this arc (shown in Figure 4.36). At this temperature the higher frequency arc was found to be incomplete.

The double arc in Figure 4.35 implies a minimum of two “phases” and a possible third phase, present in the SSiC material. XRF analysis performed on this material showed that this sample did only contain Si and C. If SiC were the only phase in the material, then one would expect to only see one arc in the Cole-Cole plot. The Cole-Cole plots confirm that there are at least two phases or grain boundary materials giving rise to the Cole-Cole plots.

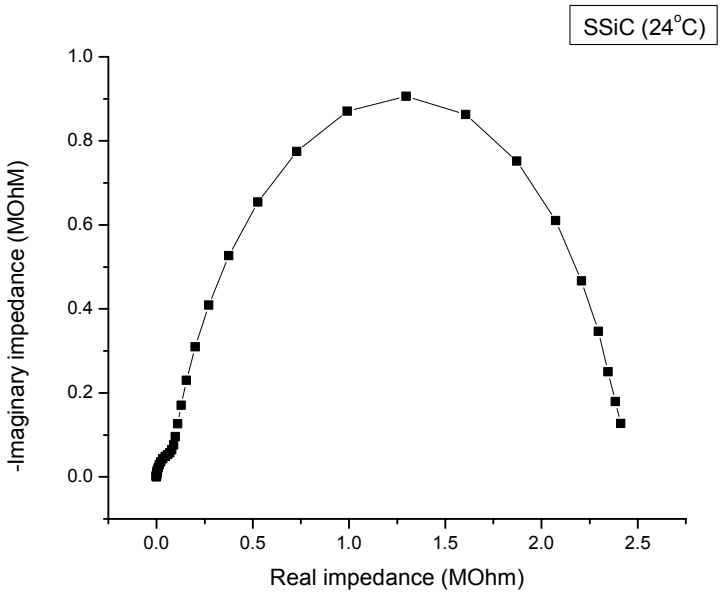


Figure 4.35 Cole-Cole plot for the SSiC material at room temperature

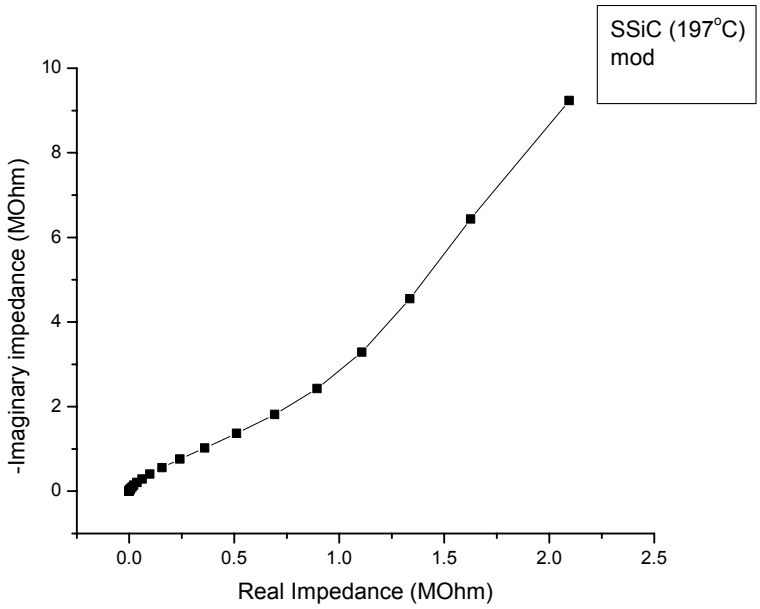


Figure 4.36 Cole-Cole plot for the SSiC material at liquid nitrogen temperature (-196°C)

The HP0.7YS material, exhibited variable range hopping conductivity (seen in Table 4.20). Since this material was only 88 % dense and contained high open porosity (about 5 %), it was not included when discussing and comparing all the dense HP and GPS systems sintered with Y_2O_3 and Al_2O_3.

In the measurements of the 4 mass-% GPS $1Y_2O_3$:$4Al_2O_3$ material, GP1Y4Al_4, which was pressureless sintered to full density, there was a lot of noise in the results, so these measurements are not presented. Also, the two ac instruments and dc instrument did not agree with each other. Only one arc could be distinguished in the Cole-Cole plots for this material.